AAEC/E327

AAEC/E327

AUSTRALIAN ATOMIC ENERGY COMMISSION

RESEARCH ESTABLISHMENT

LUCAS HEIGHTS

keV NEUTRON RESONANCE CAPTURE IN BARIUM-135

by

A. R. deL. MUSGROVE

B. J. ALLEN

R. L. MACKLIN *

* Oak Ridge National Laboratory, Oak Ridge, Tennessee, USA

Research sponsored in part by the USAEC under contract to
Union Carbide Corporation

December 1974

ISBN 0 642 99667 9

AUSTRALIAN ATOMIC ENERGY COMMISSION
RESEARCH ESTABLISHMENT
LUCAS HEIGHTS

keV NEUTRON RESONANCE CAPTURE IN BARIUM-135

by

A.R. deL. MUSGROVE
B.J. ALLEN
R.L. MACKLIN*

ABSTRACT

The neutron capture cross section of ^{135}Ba has been measured with high resolution at the Oak Ridge Linear Accelerator in the energy range 3 to 100 keV. From over ninety observed resonances in the 3 to 6 keV energy range, the average resonance parameters obtained were: $\langle \Gamma_\gamma \rangle$ = 150 ± 20 meV; $\langle D \rangle$ = 39.3 ± 4 eV and $10^4 S_1$ = 0.8 ± 0.2. The quoted radiation width and p-wave strength function also have a normalisation error of ± 20 per cent. The method of separation of s- and p-wave populations by statistical methods is described.

* *Oak Ridge National Laboratory, Oak Ridge, Tennessee, USA.*
Research sponsored in part by the USAEC under contract to Union Carbide Corporation.

National Library of Australia card number and ISBN 0 642 99667 9

The following descriptors have been selected from the INIS Thesaurus to describe the subject content of this report for information retrieval purposes. For further details please refer to IAEA–INIS–12 (INIS: Manual for Indexing) and IAEA–INIS–13 (INIS: Thesaurus) published in Vienna by the International Atomic Energy Agency.

BARIUM 135; CAPTURE; CROSS SECTIONS; ENERGY LEVELS; KEV RANGE 01–10; KEV RANGE 10–100; MONTE CARLO METHOD; NEUTRON REACTIONS; P WAVES; RESONANCE; S WAVES

CONTENTS

1. INTRODUCTION

The neutron capture cross sections of separated isotopes of barium (^{134}, ^{135}, ^{136}, ^{137}, ^{138}Ba) were measured at the Oak Ridge Electron Linear Accelerator (ORELA) facility; the data obtained are being analysed in detail at Lucas Heights to yield information on the s- and p-wave neutron resonance parameters and on the neutron capture cross sections in the region 3 to 100 keV. Preliminary results of this analysis were reported recently at the Soviet National Conference on Neutron Physics (Allen *et al.* 1973a), and the earlier results are now superseded. The present report gives details of the analysis of the ^{135}Ba capture data with the techniques used to discriminate between s- and p-wave levels. The resulting s-wave levels have average level spacing in excellent agreement with that found at low energy by other experimenters. The most probable p-wave neutron strength function is deduced from the neutron widths extracted from the assumed p-wave levels.

2. EXPERIMENTAL DETAILS

The details of the experimental arrangement and equipment have already been extensively documented (Macklin 1971, Macklin & Allen 1971, Allen *et al.* 1973b). In brief, this measurement was performed at the 40 m station of ORELA. The capture γ-rays were collected by a total energy detector with efficiency independent of the nature of the γ-ray spectrum. A calculated pulse height weighting scheme ensures that, on average, the detector response is proportional to the total energy of the event (*i.e.* the binding energy plus the centre of mass neutron bombarding energy).

For each event detected, a weight (GWT) - actually an energy weight - is obtained from the calculated table and is then added into the appropriate time channel file along with its variance. Finally, the number of capture events at energy E is obtained from:

$$N_C(E) = \frac{GWT\ (E)}{E_B + EA/(A+1)} \quad ,$$

where E is the neutron kinetic energy and GWT (E) is the cumulated product of weight and total energy at the time channel corresponding to E. The denominator is the total energy of the capture events in this channel.

The experiment described here was performed earlier than the lead runs already published (Allen *et al.* 1973b). In that paper, a description of the thin (0.5 mm) ^{6}Li glass neutron flux monitor is given. The glass is inserted in the neutron beam at 39 m and provides, *via* the ^{6}Li (n,α) cross section (Uttley *et al.* 1971), a direct contemporary measure of the incident neutron

flux. For early measurements such as the one here described, a time-gated communal fission detector measures the time integrated neutron yield at the source (assumed to be proportional to the integrated flux at 40 m).

After installation of the ^{6}Li glass, the ^{6}Li (n,α) yield was measured (along with the number of fission counts), and the barium results can be normalised to the ^{6}Li (n,α) cross section by using the ratio of the two fission counts. It is believed that the normalisation, relying on the fission monitor alone, is no more than 30 per cent accurate over long time periods. Fortunately for the ^{135}Ba run, a secondary standard is available. Two runs on gold were performed directly after the barium-135 run and, when these runs are normalised to the ^{6}Li yield *via* the fission counter, the cross section in the keV region can be compared with previous measurements. For the gold runs we obtain at 30 keV:

Run 1 Au σ(exp)/σ(standard) = 1.04 ± 30 per cent

Run 2 Au σ(exp)/σ(standard) = 0.96 ± 30 per cent

where the 30 per cent error is the expected long time-scale normalisation error.

From these gold results and also from the lead results (Allen *et al.* 1973b) it is claimed that, for short time periods, the normalisation achieved with the fission monitor is reproducible to within about 10 per cent.

Summarising the above argument then, the normalisation to the much later ^{6}Li (n,α) yield is expected to be accurate to about 30 per cent. However, the results could have been normalised to the subsequent gold runs with an error of about 10 per cent. Taking a pessimistic view, a 20 per cent error is assumed in the normalisation to the ^{6}Li (n,α) cross section, which is believed to be known to better than 2 per cent below 100 keV.

The target consisted of an enriched (93.6 per cent) sample of $^{135}Ba\,CO_3$ containing 14.27 g of ^{135}Ba. The target thickness was 0.0061 atoms/barn with linear dimensions 2.61 x 2.61 x 0.84 cm.

The accelerator operated with a pulse width of 5 ns giving 26.8×10^{8} bursts during the run, while 1.06×10^{6} fissions were counted on the fission monitor.

3. DATA REDUCTION

At the completion of the capture measurement (about one day's running time) the data are dumped on tape for further analysis. Routine dead time and time independent background corrections are made and the GWT data, originally in time channels, are transformed to an energy scale. The data are then converted to a capture yield (in mb) *via* the fission counter and later ^{6}Li monitor yields as previously described. The data still contain a

time dependent background and have not been corrected for self shielding and multiple scattering. The ^{135}Ba capture yield data at this stage are displayed in Figure 1 for the energy region 3 to 90 keV. Also indicated is the background (assumed linear in each region) along with its assumed error.

4. ANALYSIS

4.1 Area Analysis Using Monte Carlo Method

A modified version of the RPI Monte Carlo code (Sullivan *et al.* 1969, plus later errata) is used extensively in the analysis of capture experiments. The code uses initial guesses for the resonance neutron and radiative widths for up to ten resonances at a time, and calculates the multiple scattering component of the capture yield. This component is subtracted from the experimental yield and the code then performs an iterative area fit to each resonance which is assumed to sit on a linear background. For ^{135}Ba between 3 to 6 keV we examined 100 channel segments (100 eV) of the data in turn which contain, on average, about three resonances to be fitted. The calculated primary capture yield at each resonance is convoluted with the resolution function, and the shape fit to the data is examined visually (at the end of the iteration, the capture areas should be equal). It is claimed that the FWHM of the resolution function is known very accurately as a function of energy by Gaussian width fitting of many large unresolved (*i.e.* with $\Gamma \ll$ resolution width) resonances in this nucleus. The Doppler broadening width is, of course, added in quadrature to the resolution width.

Experience with other isotopes has shown that resonances with widths down to about 0.5 resolution widths can be resolved. That is, as well as an area fit, a shape fit to the resonance can also be performed to extract Γ_n. For resonances with widths smaller than this limit, no detectable Breit-Wigner tail can be discerned, nor the consequent reduction in resonance peak height.

For ^{135}Ba, most resonances fall into the latter category and only one resonance can be resolved out of the 90 observed.

The quantity obtained from the area fit is the idealised thin sample capture area:

$$A_\gamma = 2\pi^2 \lambda\!\!\!^{-2}\, g\, \Gamma_n \Gamma_\gamma / \Gamma \quad ,$$

and it is assumed that the reader is familiar with the conventional meanings of these terms. The amount of self shielding occurring due to finite thickness of the target is calculated in the programme and, for the largest resonances in ^{135}Ba, this effect reduces the capture yield by a factor of

about 0.7 to 0.8 of the thin target yield. This self shielding effect predominates over the (negligible) multiple scattering correction for this nucleus at the energies considered here. For the smaller resonances the self shielding correction rarely exceeds 5 per cent.

4.2 The Resonance Parameter Kernel

The resonance parameter kernel of A_γ is also of interest. This quantity is denoted by:

$$\kappa = g\Gamma_n\Gamma_\gamma/\Gamma \text{ (eV)} \quad .$$

When the programme is iterating to determine A_γ, it alters either Γ_n or Γ_γ, whichever is the smaller. Therefore, for small resonances where $\Gamma_n \ll \Gamma_\gamma$ a value for Γ_γ is put into the programme which will not be altered by the fitting procedure. For very small resonances, $\kappa \simeq g\Gamma_n$ and this is the output quantity.

For the larger resonances having $\Gamma_n > \Gamma_\gamma$, a nice separation of κ into two groups corresponding to the two g values for s-neutrons is expected. For ^{135}Ba, which has target spin of $^3/_2^+$, the g values are sufficiently different (0.625 and 0.375) to make J assignments with some confidence. Of course, it must be assumed that Γ_γ is independent of J in order to do this.

More qualitatively, from the previously published low energy information on this nucleus (Van der Vyver & Pattenden 1971, Alves *et al.* 1968) may be taken estimates of the average resonance parameters as follows: $S_o \simeq 1.0 \times 10^{-4}$, $\langle D \rangle \simeq 40$ eV and $\langle \Gamma_\gamma \rangle \simeq 100$ meV. A rough estimate of the average s-wave neutron width at 3 keV based on these parameters is 0.4 eV, or about 4 times the radiation width. From Porter-Thomas statistics, some 60 per cent of the s-wave levels will have neutron widths larger than their radiative widths. On the other hand, the resolution FWHM at 3 keV is 5 eV increasing to 10 eV at 6 keV. Thus, it is extremely unlikely that any resonances will be resolved. In fact, the 4,629 eV resonance is just resolved with $\Gamma_n = 6.0$ eV, but for no other large s-wave level can a reasonable estimate of Γ_n be made.

4.3 Example of Analysis on the 3,199 eV Resonance

In Figure 2 is given a typical example of a detailed Monte Carlo area analysis performed on the 3,199 eV resonance. The resonance Γ_n has been varied from 0.2 eV to 2.0 eV. At $\Gamma_n = 2.0$ eV, the Breit-Wigner tail of the resonance and the compensating drop in the peak height makes the visually inspected shape fit to the resonance discernibly worse than with $\Gamma_n = 1.0$ eV.

For all Γ_n values $\leq$ 1.0 eV, the resonance shape is fitted very well. From Figure 2(a) it can be seen that Γ_γ remains close to 150 meV for Γ_n values in the range 0.8 to 0.4 eV before beginning to increase sharply as Γ_n approaches Γ_γ.

The behaviour of the self shielding factor as a function of Γ_n, shown in Figure 2(b), is typical of the large s-wave levels and the effect which this produces on the true resonance capture area is displayed in Figure 2(c). To obtain the resonance parameters for Table 1, a number of different approaches are possible. For example, the expectation value of the unknown capture area is presumably an average over the Porter-Thomas Γ_n distribution. To perform such an average, a value for $\langle \Gamma_n \rangle$ would be required, but also, while such an approach may be sound mathematically, it is readily seen in Figure 2(a) that the average would actually weight highly a region (with Γ_n close to 0.2) which may be judged to be physically unlikely. That is, for this region the radiation widths are much larger than the mean radiation width obtained for this nucleus. In the event, the radiative width for this resonance is estimated to be $\Gamma_\gamma \gtrsim 150$ meV and a somewhat arbitrary value has been taken for Γ_n of 0.4 eV to obtain the capture area indicated in Figure 2(c) with the error associated with this estimate. It is felt that this procedure can at least be more readily corrected if further measurements are made on this nucleus.

For the analysis of the 3,199 eV resonance, it was assumed J = 2 and hence g = 0.625. Had J = 1 been assumed for this resonance, the curve in Figure 2(a) would be shifted considerably to the right (*i.e.* to much higher Γ_γ values). The lower value was judged to be more likely and this level was assigned to the J = 2 sequence on that basis.

4.4 Separation of g Values

In the course of the present analysis, the higher g value has been assumed whenever $\kappa \geq 0.055$ eV and the appropriate J value has been given in Table 1. In the range 3 to 5 keV, 15 levels have been assigned as J = 2 and 8 as J = 1 in satisfactory agreement with a 2J+1 level density law. Of course, as shown in Figure 2(c), the resonance area and hence κ varies with Γ_n. Borderline cases therefore require a physical assessment of which J value seems more likely, and to this extent, may be regarded as uncertain. To further amplify this problem, reference is made to the group of levels near 5.1 keV. These six large resonances look identical in the capture cross section and would, on the basis of their apparent κ values, be all assigned to the J = 1 sequence. Clearly this is not a physically possible interpretation, bearing in mind the Wigner distribution's injunction against small spacings of levels of the same

spin sequence. The first level of this group was analysed as J = 1 and the remainder have been analysed assuming g = 0.5 and are not assigned to either sequence.

4.5 Average Parameters

Although each particular resonance A_γ suffers from the uncertainty in Γ_n, the average cross sections as finally presented in Figure 9 contain contributions from a number of large s-wave levels (indicated by * in Table 1) and the authors are confident that the error on the final average cross section, due to the lack of knowledge of any particular resonance Γ_n, is small compared with the overall normalisation error. A similar observation applies to the final best estimate for the average radiative width for this nucleus. From the eight large resonances, between 3 and 4 keV $\langle \Gamma_\gamma \rangle$ can be estimated to be 150 meV with an estimated error of ± 20 meV. The resolved resonance at 4,629 eV has Γ_γ = 135 ± 15 meV which agrees with this value within the errors.

Clearly, the resonance parameters presented in Table 1 are not the result of a 'once through' analysis. Above has been indicated the sort of analysis required to obtain an estimate for $\langle \Gamma_\gamma \rangle$ for this nucleus from those resonances having the largest capture areas (and presumably $\Gamma_n > \Gamma_\gamma$). In this energy region, and with a believable value for the p-wave neutron strength function, it can be calculated that these are (almost) certainly s-wave levels. From the earlier rough calculation, about 60 per cent of the s-wave levels are expected to be found at this stage, however all indications show that many p-wave levels have also been detected amongst the remaining small levels. For example, far too many small values of $g\Gamma_n$ are obtained than would be expected from Porter-Thomas statistics. Also, an examination of the distribution of level spacings compared with the expected Wigner distribution (for two s-wave level sequences) shows too many small spacings. The detectability limit in the energy range covered increases approximately as E^2, which means that for the small p-wave levels (with capture area $\propto g\Gamma_n$), the best chance of observing them is at low energy (*i.e.* near 3 keV). Also, at low energy it is more easy from a calculation of the relative probabilities to decide if a level is more likely to be s-wave or p-wave.

4.6 Bayes' Theorem Analysis

In this section the workings of such a calculation, usually termed a 'Bayes' theorem analysis', are examined.

A resonance occurs at energy E with capture kernel $g\Gamma_n\Gamma_\gamma/\Gamma$ in the range $\kappa \pm \Delta\kappa$. Assuming the level to have been formed by either s- or p-wave inter-

action gives 6 possible (ℓ,J) sequences (mutually exclusive) to which the level can belong. Estimates are required of S_o and S_1, the s- and p-wave neutron strength functions, $\langle D \rangle$, the s-wave level spacing and, Γ_γ, the average radiation width. The average reduced neutron widths can be calculated for each of the 6 (ℓ,J) sequences:

$$\langle \Gamma^{\ell}_{nJ} \rangle = S_{\ell} \frac{\langle D \rangle}{g} \varepsilon^{\ell}_{IJ}$$

where ε^{ℓ}_{IJ} is the number of channel spin contributions (either 1 or 2). Now for each sequence the quantity $\kappa \pm \Delta\kappa$ is transformed to a corresponding $\Gamma_{nJ} \pm \Delta\Gamma_n$, and this is further reduced to the reduced neutron width $\Gamma^{\ell}_{nJ} \pm \Delta\Gamma^{\ell}_{n}$ by dividing by the ℓ-wave penetration factor and $\sqrt{E}$. If $\varepsilon^{\ell}_{IJ} = 1$, the neutron widths come from a Porter-Thomas distribution, while when $\varepsilon^{\ell}_{IJ} = 2$, which occurs for two of the p-wave sequences, the neutron widths come from the χ^2_2 or negative exponential distribution. The probability of finding Γ^{ℓ}_{nJ} in the specified error range is now readily calculated and the result of this is further multiplied by the *a priori* density factor $\rho_J = 2J+1$. The probabilities so calculated are finally normalised such that the sum is unity and the probability that the level in question is either s-wave or p-wave is found. In Figure 3 this calculation is illustrated with the final best estimate parameters for E = 3 keV and E = 6 keV. For each value of κ are shown the calculated probabilities for a level to belong to each of the six (ℓ,J) sequences. The s/p wave boundary is shown as a heavy line. Utilising these figures, it is seen that the group of four levels designated p-wave near 3.1 keV have $\kappa \leqslant 0.007$ which, by reference to Figure 3, gives $\lesssim 15$ per cent probability that these are s-wave. This is about the level at which the 'clear cut' decision to call these p-wave resonances operates. Others who use a similar technique to separate small p-wave levels (*e.g.* Bollinger & Thomas 1968, Thomas *et al.* 1972, Liou *et al.* 1972a) are able to achieve much greater confidence levels for their separations since they operate at lower energies.

4.7 Statistical Tests

In addition to separating a p-wave component in the manner described above, further checks have been made which can be applied to the remnant s-wave population. Statistical tests which can be applied to a single sequence (*i.e.* one ℓ,J value) have been reported by Liou *et al.* (1972b) and are used extensively by the Columbia group in their analyses. In ^{135}Ba there are two s-wave sequences, and there is the further problem caused by missing levels from the main sequence. In the circumstances, the s-wave level spacing data

are tested against the expected 2J+1 weighted Wigner distribution for two sequences and, since many of the neutron widths for these levels are unknown, tests can only be made to ensure that the number of small s-wave levels is approximately correct, assuming the value $S_o = 1.0 \times 10^{-4}$ recommended by Van der Vyver & Pattenden (1971).

5. RESULTS

Finally, the staircase plot of s-wave levels is obtained (Figure 4). An average spacing of 41 eV is indicated from a straight line fit to the lower portion of this staircase, and the distribution of spacings about this average is given in Figure 5 compared with the expected distribution. This plot shows that 4 to 5 small spacings are missing and a similar number appear to be missing from the staircase plot between about 4 and 6 keV. It would be a mistake to assume that these missing levels are simply misassigned p-wave levels, although some misassignments have undoubtedly occurred in this analysis. Overlapping of s-wave levels can occur, although the only likely candidate seems to be the level at 5,978 eV which has a very large value of κ. The most probable reason for missing s-wave levels is simply that the detectability limit increases faster than the resonance area for the smallest s-wave levels and, therefore, at 6 keV some s-wave levels are below the limit of detectability.

Using the low energy levels found by Van der Vyver & Pattenden (1971) the level spacing has also been evaluated for this nucleus. Their speculative 26.0 eV resonance was omitted from this evaluation shown in Figure 6, and the best estimate for the level spacing in ^{135}Ba was found to be 39.3 ± 3.0 eV.

In Figure 7, the quantity κ is plotted for all resonances observed *versus* neutron energy. The transverse line marks the boundary, calculated by the Bayes' theorem analysis, at which a level has equal *a priori* probability of being s-wave or p-wave. This boundary has been calculated with the final best set of average parameters. The position of this boundary is quite a sensitive function of the parameters, in particular, the p-wave strength function and the average radiation width.

Figure 8 gives the cumulative sum of $g\,\Gamma_n^l$ *versus* neutron energy for this nucleus. A straight line fit to the slope here has produced a strength function estimate of $\sim 0.6 \times 10^{-4}$; however, taking into account the large number of p-wave levels missed (only 25 versus 68 s-wave levels are seen), a value $S_1 = 0.8 \pm 0.2 \times 10^{-4}$ is estimated for this nucleus.

Finally, the capture cross section in the energy range 3 to 90 keV has been obtained. From 3 to 6 keV the cross section is almost entirely subscribed

by the observed resonances, but above 6 keV the cross section has been obtained by integrating the capture yield in each region, subtracting a linear background (shown in Figure 1) and then making an average self shielding and multiple scattering correction using the approximation of Macklin (1964). In this process, the background subtraction is the major source of error as shown in Figure 9. The normalisation error has not been included. Also shown in Figure 9 is the calculated statistical model cross section using the best set of average resonance parameters. The fit is good and tends to lend some support to the p-wave strength function, which was derived as described from resolved resonances near 3 keV yet still fits the cross section in regions where the p-wave contribution exceeds the s-wave contribution.

6. CONCLUSION

The measured radiative width is larger than that found by early workers at low energy (Van der Vyver & Pattenden 1971, Alves *et al.* 1968). They report values around 100 meV and this may point to a normalisation error in the present results. On the other hand, the weighted contribution of the ^{135}Ba capture cross section to the measured natural element cross section at an energy of 61 ± 5 mb (Macklin *et al.* 1963) is 20 ± 7 mb. This is by far the major contribution to the natural element cross section and can scarcely be reduced. The preliminary results for the other isotopes to date give a calculated elemental cross section of only 38 ± 10 mb.

7. REFERENCES

Allen, B.J., Chan, D.M.H., Musgrove, A.R.deL. & Macklin, R.L. (1973a) - Proceedings of Soviet National Conference on Neutron Physics, Kiev 1973.

Allen, B.J., Macklin, R.L., Winters, R.R. & Fu, C.Y. (1973b) - Phys. Rev., C8 (4) 1504.

Alves, R.N., de Barros, S., Chevillon, P.L., Julien, J., Morgenstern, J. & Samour, C. (1969) - Nucl. Phys., A134 : 118.

Bollinger, L.M. & Thomas, G.E. (1968) - Phys. Rev., 171 (4) 1293.

Liou, H.I., Camarda, H.S., Wynchank, S., Slagowitz, M., Hacken, G., Rahn, F. & Rainwater, J. (1972a) - Phys. Rev., C5 (3) 974.

Liou, H.I., Camarda, H.S. & Rahn, F. (1972b) - Phys. Rev., C5 (3) 1002.

Macklin, R.L., Gibbons, J.H. & Inada, T. (1963) - Phys. Rev., 129 : 2965.

Macklin, R.L. (1964) - Nucl. Instrum. Methods 26 : 213.

Macklin, R.L. (1971) - Nucl. Instrum. Methods 91 : 79.

Macklin, R.L. & Allen, B.J. (1971) - Nucl. Instrum. Methods 91 : 565.

Sullivan, J.G., Warner, G.G., Block, R.C., & Hockenbury, R.W. (1969) - RPI-328-155.

Thomas, G.E., Bollinger, L.M. & Cote, R.E. (1972) - Nucl. Phys., A193 : 643.

Uttley, C.A., Sowerby, M.G., Patrick, B.M. & Rae, E.R. (1971) - Proceedings of 3rd Conference on Neutron Cross Sections and Technology, Knoxville, 1971, p.531.

Van der Vyver, R.E. & Pattenden, N.J. (1971) - Nucl. Phys., A177 : 393.

TABLE 1

FINAL RESONANCE PARAMETERS FOR ^{135}Ba

Resonance	Energy keV	$g\Gamma_n\Gamma_\gamma/\Gamma$ eV	Area BeV	Statistical Error in Area %		ℓ	J	$g\Gamma_n$ eV	Γ_γ meV	$g\Gamma_n^0$ eV	$g\Gamma_n^1$ eV
1	3.059	0.072	97.6	22	*	0	2	(0.3)	⩾ 187		
2	3.098	0.005	6.1	30		1		0.005	(150)		0.012
3	3.108	0.005	6.3	30		1		0.005	(150)		0.012
4	3.120	0.007	8.9	30		1		0.007	(150)		0.019
5	3.147	0.004	5.4	30		1		0.004	(150)		0.010
6	3.199	0.068	88.7	22	*	0	2	(0.4)	⩾ 150		
7	3.231	0.013	16.9	19		0		0.016	(150)	0.000	
8	3.277	0.028	35.7	8		0		0.045	(150)	0.001	
9	3.288	0.010	12.8	30		1		0.011	(150)		0.026
10	3.305	0.006	7.9	25		1		0.007	(150)		0.015
11	3.321	0.003	3.5	30		1		0.003	(150)		0.006
12	3.340	0.009	11.5	20		1		0.011	(150)		0.024
13	3.358	0.019	23.9	16		0		0.026	(150)	0.000	
14	3.402	0.024	29.8	10		0		0.036	(150)	0.001	
15	3.419	0.064	77.6	25	*	0	2	(0.5)	⩾ 120		
16	3.432	0.015	17.6	16		0		0.018	(150)	0.000	
17	3.464	0.014	16.5	15		0		0.016	(150)	0.000	
18	3.481	0.058	69.7	26	*	0	2	(0.5)	⩾ 116	0.000	
19	3.507	0.024	28.7	9		0		0.036	(150)	0.001	
20	3.588	0.030	34.3	13		0		0.049	(150)	0.001	
21	3.605	0.052	60.2	17	*	0	1	(0.8)	⩾ 170		
22	3.626	0.010	12.0	25		1		0.012	(150)		0.024
23	3.639	0.017	19.6	15		0		0.022	(150)	0.000	
24	3.649	0.027	30.9	15		0		0.042	(150)	0.001	
25	3.675	0.036	40.9	6		0		0.067	(150)	0.001	
26	3.710	0.030	33.4	8		0		0.049	(150)	0.001	
27	3.754	0.046	50.6	16	*	0	1	(0.8)	⩾ 145		
28	3.785	0.008	9.3	50		1		0.009	(150)		0.017
29	3.818	0.019	20.1	20		0		0.024	(150)	0.000	
30	3.826	0.024	25.9	20		0		0.035	(150)	0.001	
31	3.837	0.010	10.5	50		1		0.011	(150)		0.020
32	3.959	0.049	51.7	16	*	0	1	(0.8)	⩾ 157		
33	3.987	0.072	75.2	20	*	0	2	(0.6)	⩾ 143		
34	4.022	0.013	13.2	19		1		0.015	(150)		0.025
35	4.038	0.021	21.2	19		0		0.026	(150)	0.000	
36	4.075	0.098	99.6	19	*	0	2	(0.6)	⩾ 210		
37	4.100	0.044	44.8	15	*	0	1	(0.6)	⩾ 146		
38	4.174	0.034	33.5	16	*	0	1	(0.6)	⩾ 106		

(continued)

TABLE 1 (continued)

Resonance	Energy keV	$g\Gamma_n\Gamma_\gamma/\Gamma$ eV	Area BeV	Statistical Error in Area %		ℓ	J	$g\Gamma_n$ eV	Γ_γ meV	$g\Gamma_n^0$ eV	$g\Gamma_n^1$ eV
39	4.221	0.064	62.4	20	*	0	2	(0.6)	⩾ 122		
40	4.245	0.080	78.2	19	*	0	2	(0.6)	⩾ 161		
41	4.269	0.010	9.4	40		1		0.011	(150)		0.017
42	4.329	0.084	80.9	18	*	0	2	(1.5)	⩾ 148		
43	4.337	0.027	25.8	19		0		0.043	(150)	0.001	
44	4.361	0.010	9.6	19		1		0.011	(150)		0.017
45	4.411	0.055	51.5	19	*	0	(2)	(0.3)	⩾ 124		
46	4.443	0.112	105.0	17	*	0	2	(2.0)	⩾ 198		
47	4.464	0.009	8.1	19		1		0.009	(150)		0.014
48	4.523	0.014	13.0	19		1		0.017	(150)		0.024
49	4.568	0.036	32.8	12		0		0.066	(150)	0.001	
50	4.629	0.083	74.1	10	R	0	2	Γ_n=6.0±1	135		
51	4.677	0.022	19.9	10		0		0.031	(150)	0.000	
52	4.689	0.045	39.8	14	*	0	1	(0.4)	⩾ 170		
53	4.699	0.038	33.4	14	*	0	1	(0.6)	⩾ 120		
54	4.723	0.024	20.8	13		0		0.033	(150)	0.000	
55	4.803	0.075	65.0	18	*	0	2	(0.7)	⩾ 147		
56	4.829	0.006	5.1	19		1		0.006	(150)		0.008
57	4.850	0.010	8.5	19		1		0.011	(150)		0.015
58	4.865	0.063	54.1	19	*	0	2	(0.7)	⩾ 120		
59	4.908	0.030	25.1	16		0		0.047	(150)	0.001	
60	4.930	0.017	14.6	19		1		0.020	(150)		0.026
61	4.943	0.041	34.3	17	*	0	1	(0.3)	⩾ 172		
62	4.965	0.068	57.2	19	*	0	2	(0.4)	⩾ 166		
63	5.024	0.050	41.3	19	*	0		(0.3)	⩾ 139		
64	5.064	0.026	21.3	15		0		0.038	(150)	0.001	
65	5.076	0.046	36.3	18	*	0	1	(0.7)	⩾ 150		
66	5.100	0.043	35.0	18	*	0		(0.7)	⩾ 93		
67	5.113	0.042	34.2	18	*	0		(0.7)	⩾ 90		
68	5.150	0.050	40.1	21	*	0		(0.7)	⩾ 110		
69	5.163	0.047	38.0	25	*	0		(0.7)	⩾ 104		
70	5.172	0.048	38.2	25	*	0		(0.7)	⩾ 104		
71	5.275	0.033	26.3	13		0		0.057	(150)	0.001	
72	5.342	0.021	16.2	15		0		0.028	(150)	0.000	
73	5.357	0.065	50.3	17	*	0	2	(0.7)	⩾ 122		
74	5.414	0.053	40.4	14	*	0	1	(0.7)	⩾ 175		
75	5.448	0.067	51.0	19	*	0	2	(0.7)	⩾ 128		
76	5.500	0.061	45.8	19	*	0	2	(0.7)	⩾ 114		
77	5.525	0.025	19.1	20		1		0.033	(150)		0.036
78	5.552	0.039	29.3	15		0		0.077	(150)	0.001	

(continued)

TABLE 1 (continued)

Resonance	Energy keV	$g\Gamma_n\Gamma_\gamma/\Gamma$ eV	Area BeV	Statistical Error in Area %		ℓ	J	$g\Gamma_n$ eV	Γ_γ meV	$g\Gamma_n^0$ eV	$g\Gamma_n^1$ eV
79	5.570	0.022	16.4	19		1		0.029	(150)		0.030
80	5.593	0.069	50.9	19	*	0	2	(0.7)	$\geqslant$ 130		
81	5.620	0.046	35.2	18	*	0	1	(0.7)	$\geqslant$ 150		
82	5.659	0.020	14.9	20		1		0.025	(150)		0.026
83	5.686	0.024	17.7	20		0		0.035	(150)	0.000	
84	5.718	0.015	10.9	20		1		0.018	(150)		0.018
85	5.756	0.034	24.4	13		0		0.058	(150)	0.001	
86	5.781	0.026	18.8	13		0		0.039	(150)	0.001	
87	5.809	0.023	16.5	15		0		0.033	(150)	0.000	
88	5.842	0.014	10.2	20		1		0.017	(150)		0.028
89	5.871	0.029	20.4	20		0		0.047	(150)	0.001	
90	5.888	0.100	70.4	19	*	0	2	(0.75)	200		
91	5.905	0.070	49.1	23	*	0	2	(0.7)	140		
92	5.941	0.045	31.5	14	*	0	1	(0.7)	150		
93	5.978	0.172	119.4	14	*	0		complex peak			

* *Large s-wave levels analysed as for 3,199 eV resonance (Figure 2).*
( ) indicates assumed value.

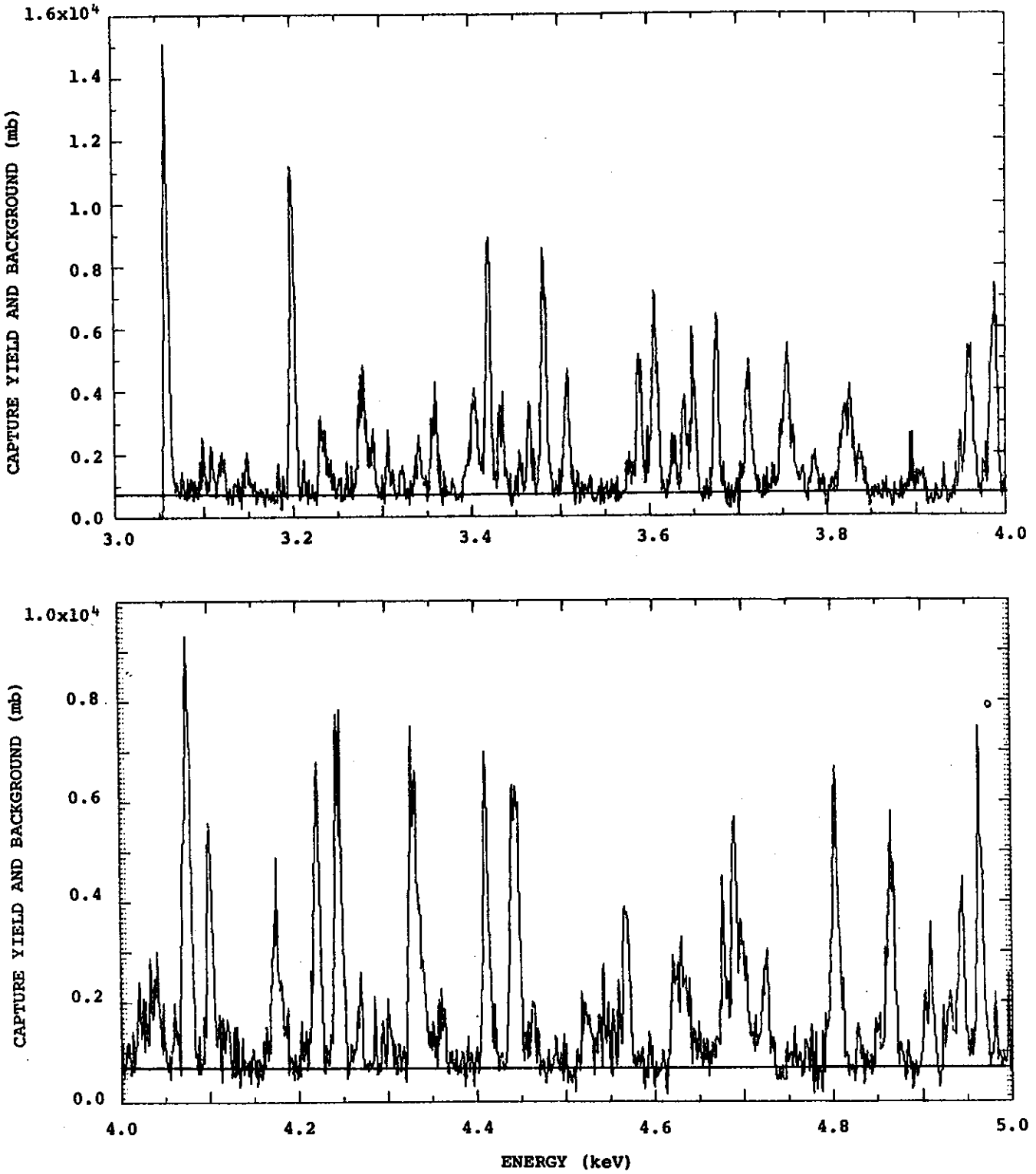

FIGURE 1(a) ^{135}Ba CAPTURE YIELD DATA 3-5 keV

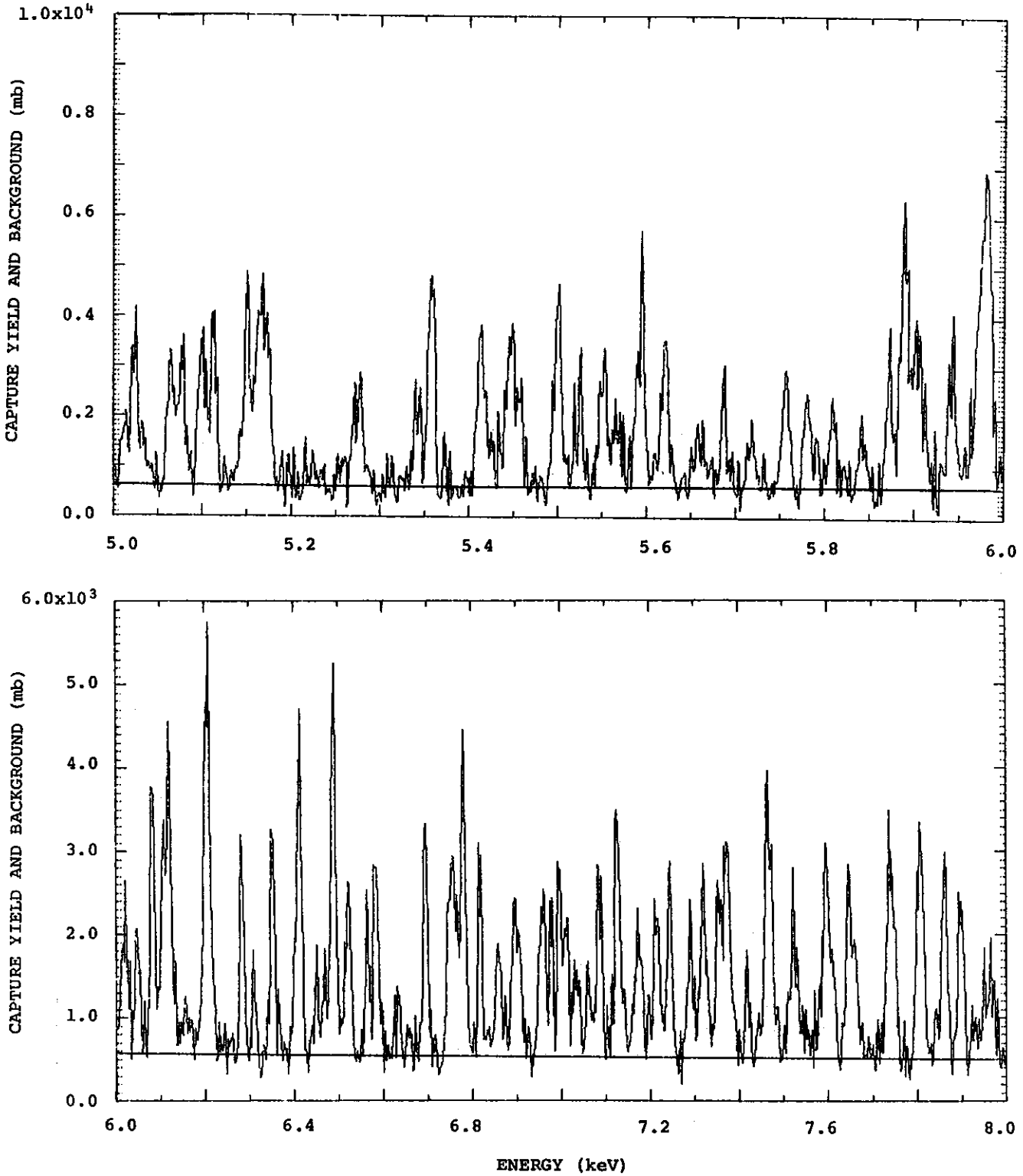

FIGURE 1(b) ^{135}Ba CAPTURE YIELD DATA 5-8 keV

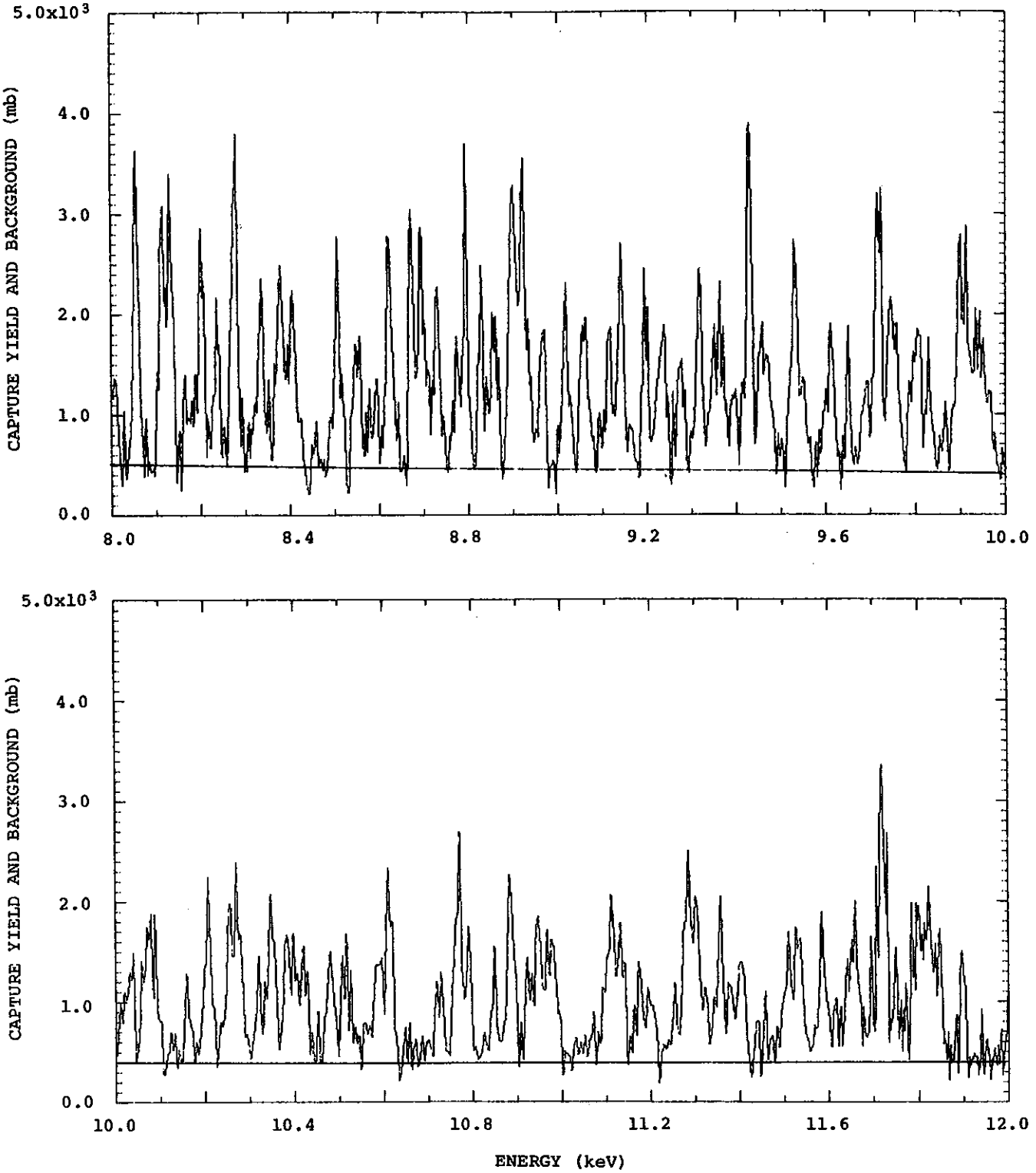

FIGURE 1(c) ^{135}Ba CAPTURE YIELD DATA 8-12 keV

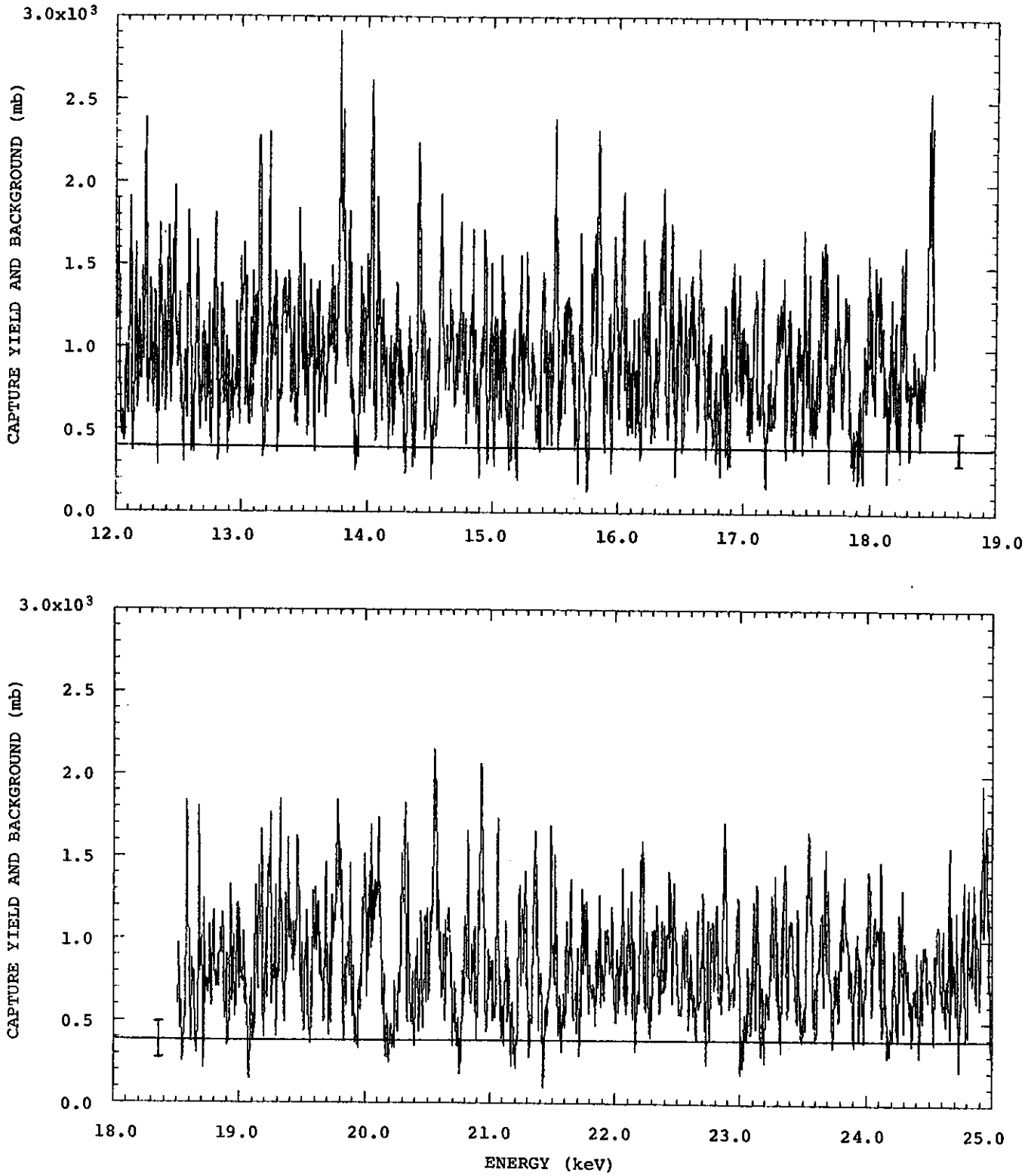

FIGURE 1(d) ^{135}Ba CAPTURE YIELD DATA 12-25 keV

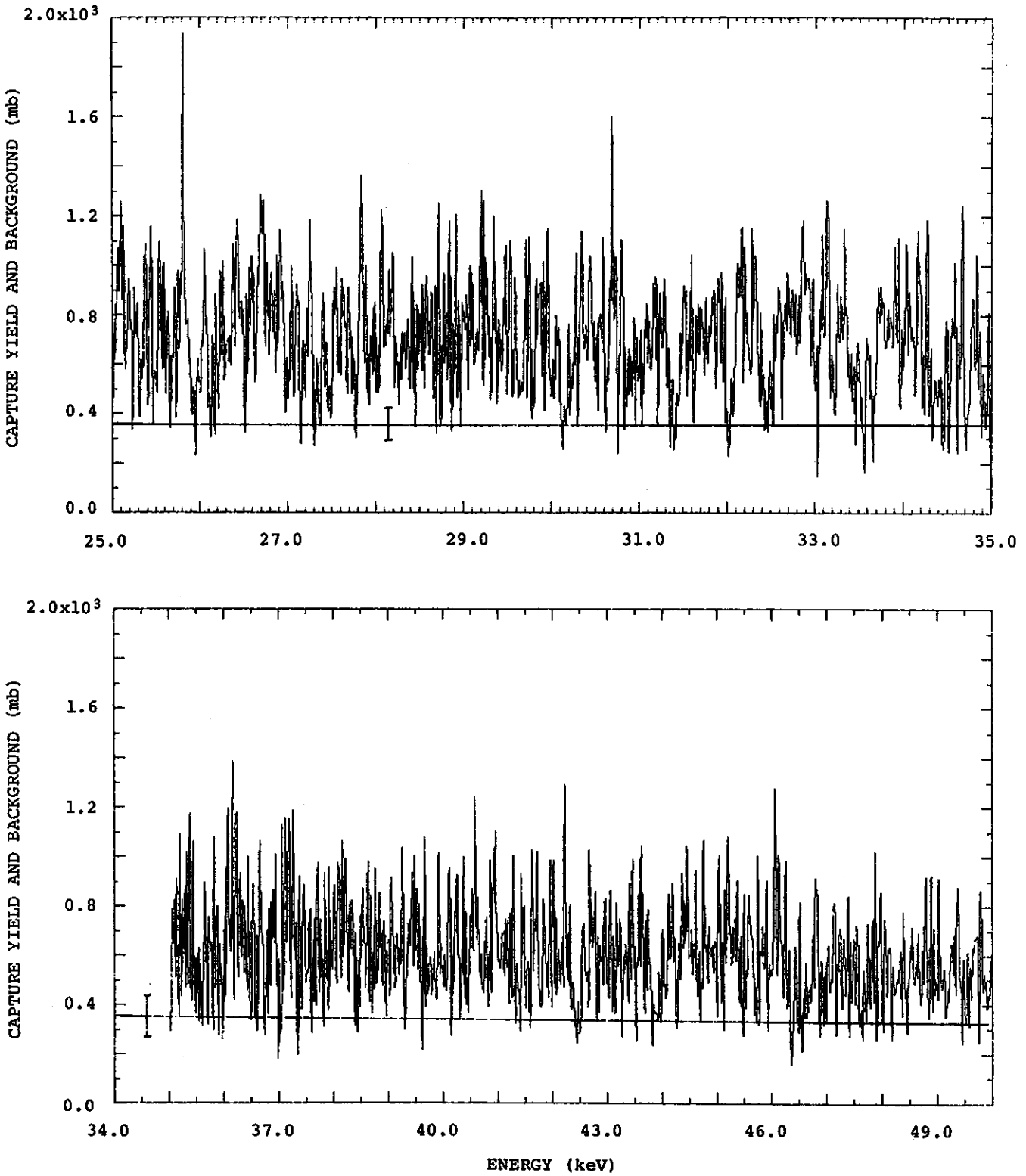

FIGURE I(e) ^{135}Ba CAPTURE YIELD DATA 25-50 keV

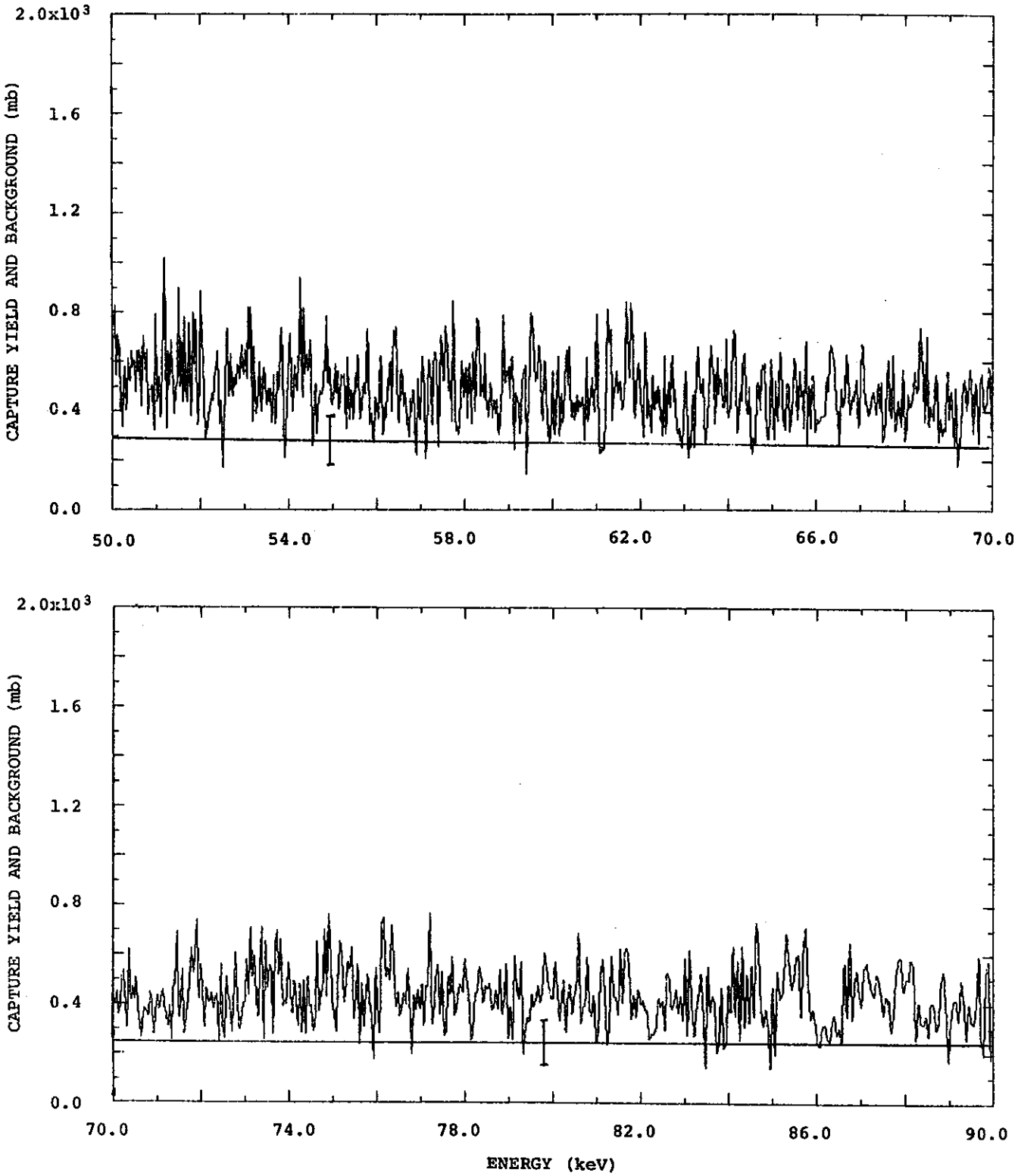

FIGURE 1(f) ^{135}Ba CAPTURE YIELD DATA 50-90 keV

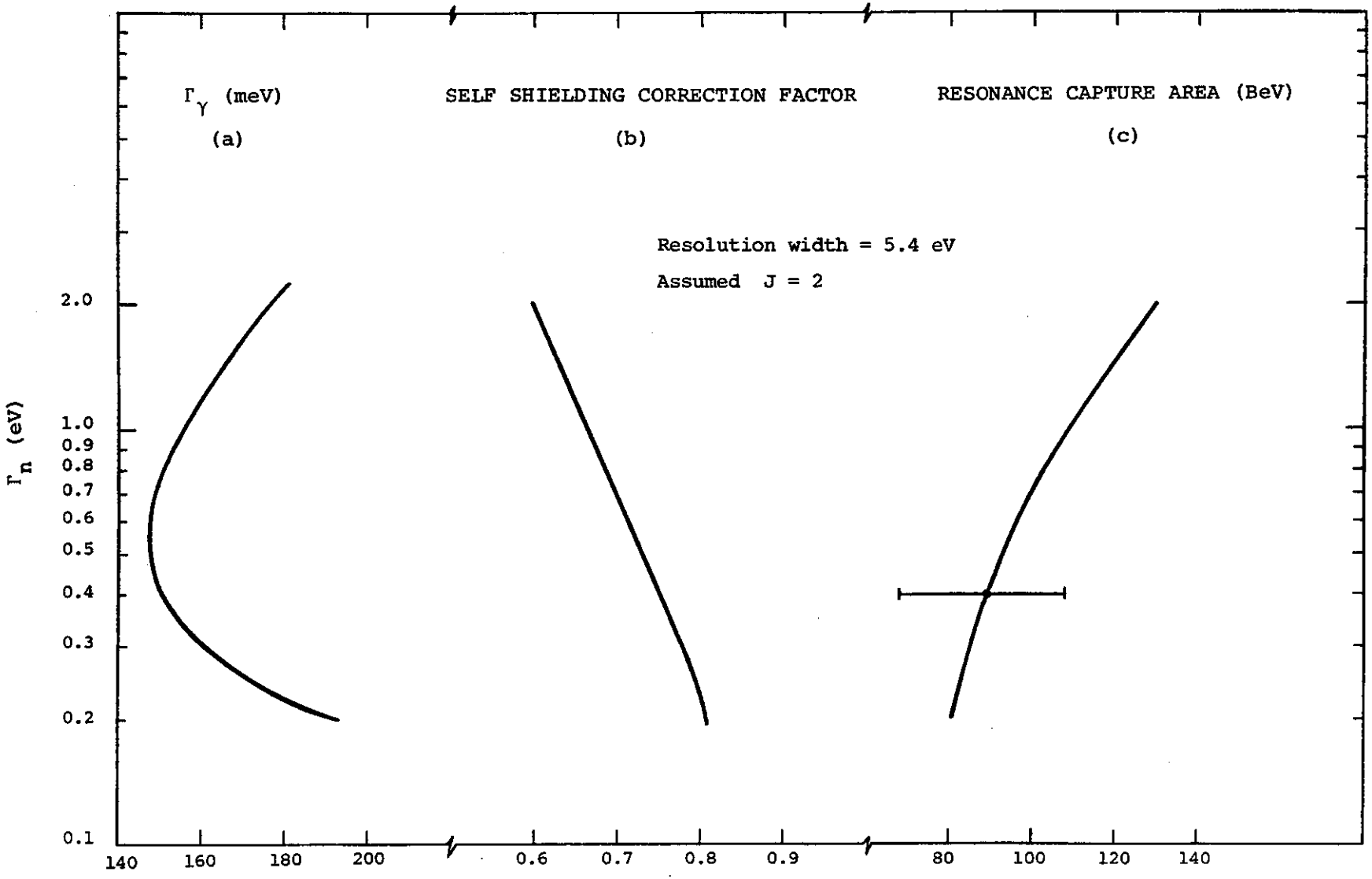

FIGURE 2. ANALYSIS OF 3199 eV RESONANCE IN ^{135}Ba.

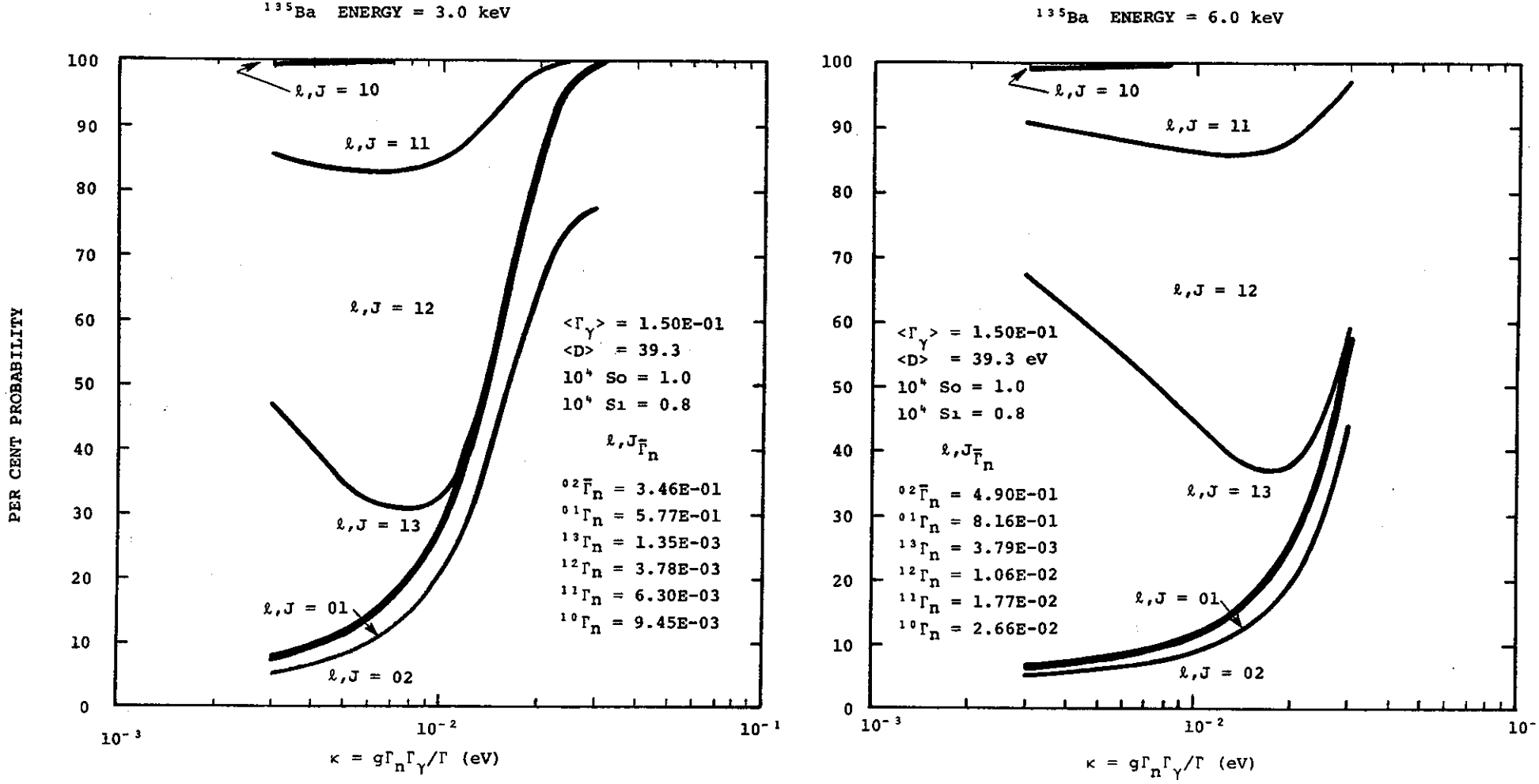

THE AREA BELOW THE HEAVY LINE REFERS TO s-WAVE LEVELS WITH ℓ,J = 01 AND 02 AS SHOWN. THE PARAMETERS USED IN THE CALCULATION ARE SHOWN

FIGURE 3. A BAYES' THEOREM ANALYSIS FOR THE PROBABILITY THAT RESONANCE WITH $g\Gamma_n\Gamma_\gamma/\Gamma = \kappa$ BELONGS TO EACH OF THE 6 POSSIBLE ℓ,J SEQUENCES IN ^{135}Ba

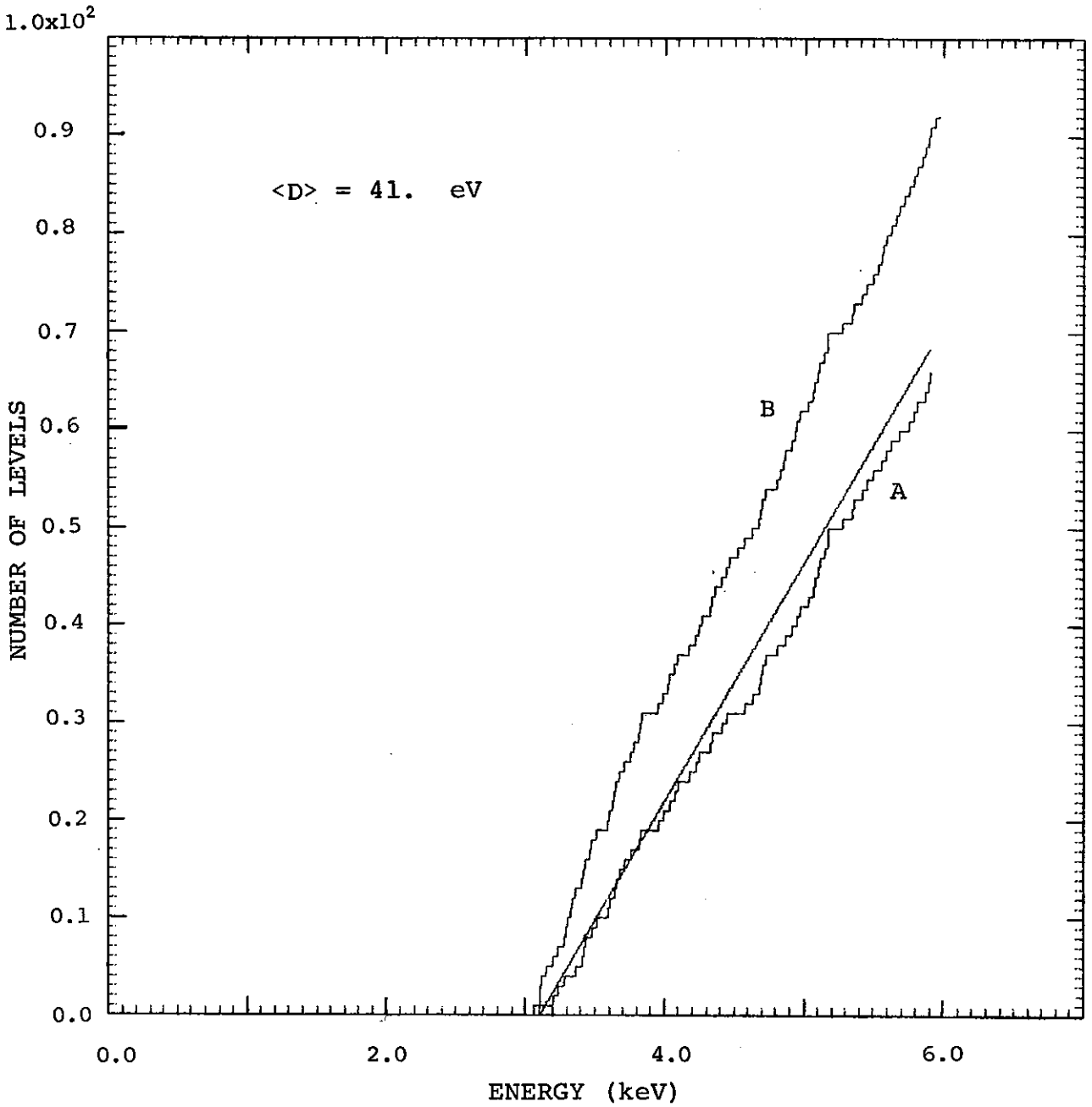

A = s-WAVE LEVELS ONLY WITH <D> = 41 eV

B = ALL LEVELS DETECTED

FIGURE 4. STAIRCASE PLOT OF NUMBER OF LEVELS UP TO ENERGY E

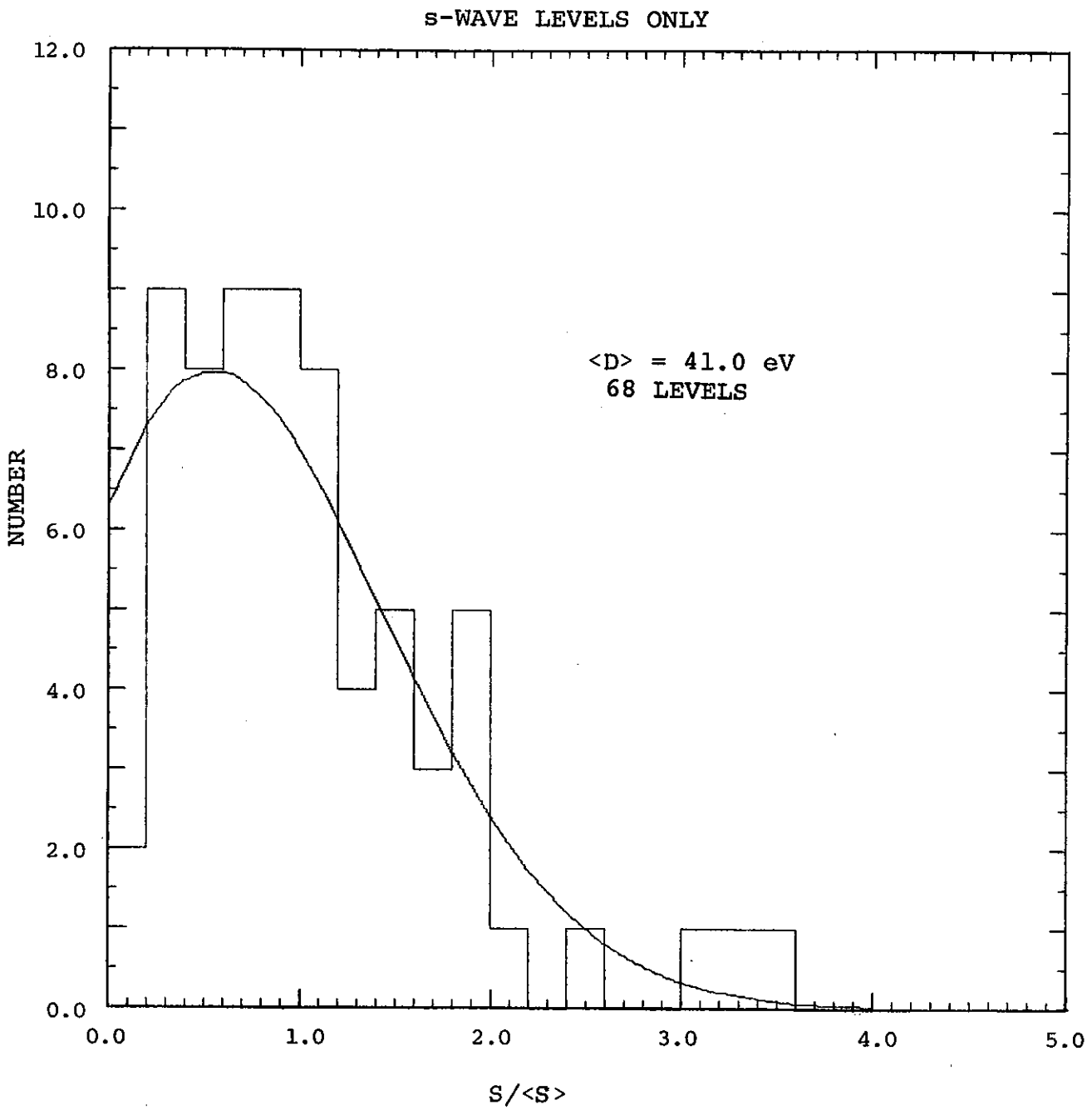

FIGURE 5. ^{135}Ba s-WAVE LEVELS COMPARED WITH A 2J+1 WEIGHTED WIGNER DISTRIBUTION

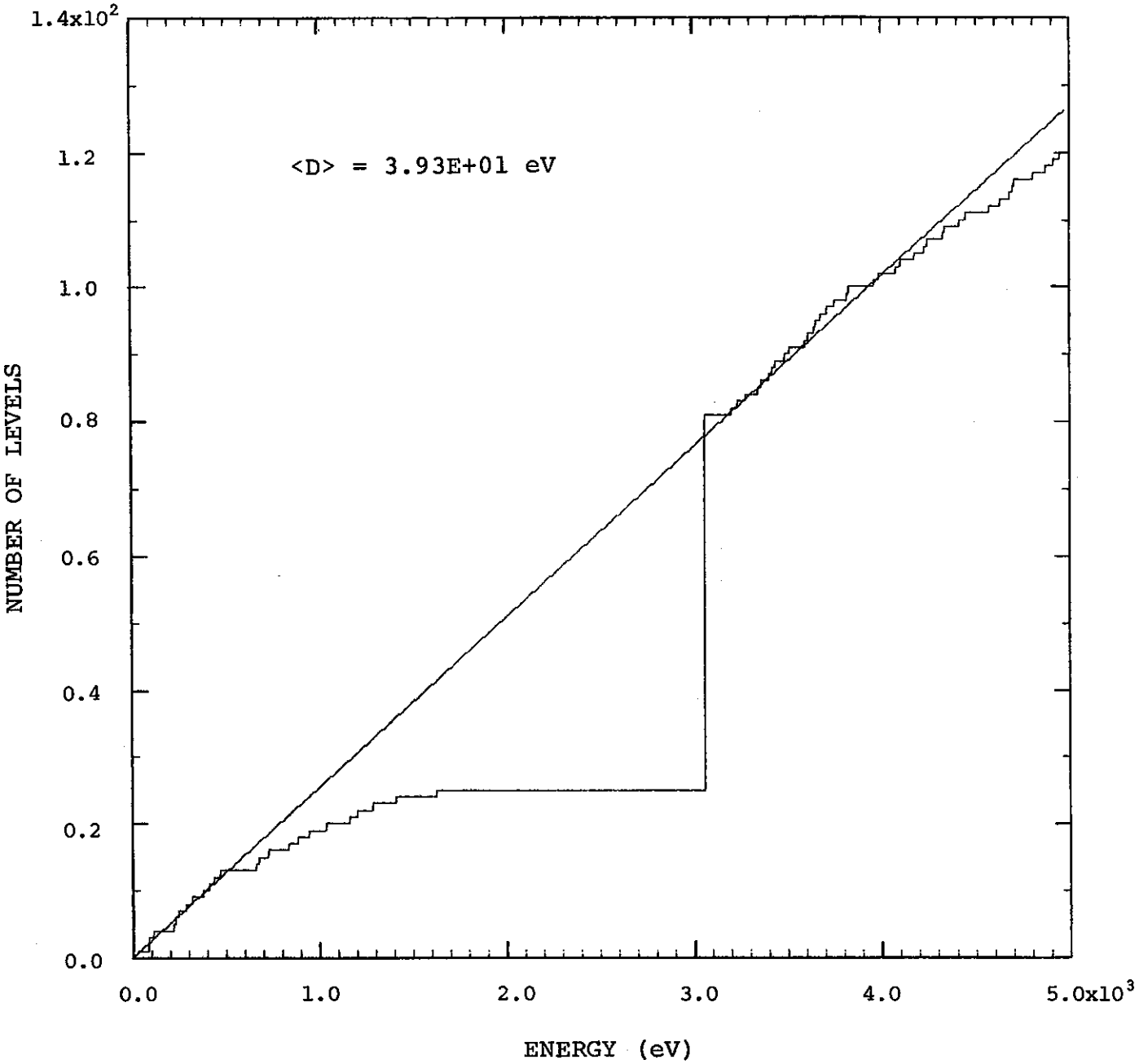

FIGURE 6. AAEC LEVEL DATA COMPARED WITH LOW ENERGY DATA

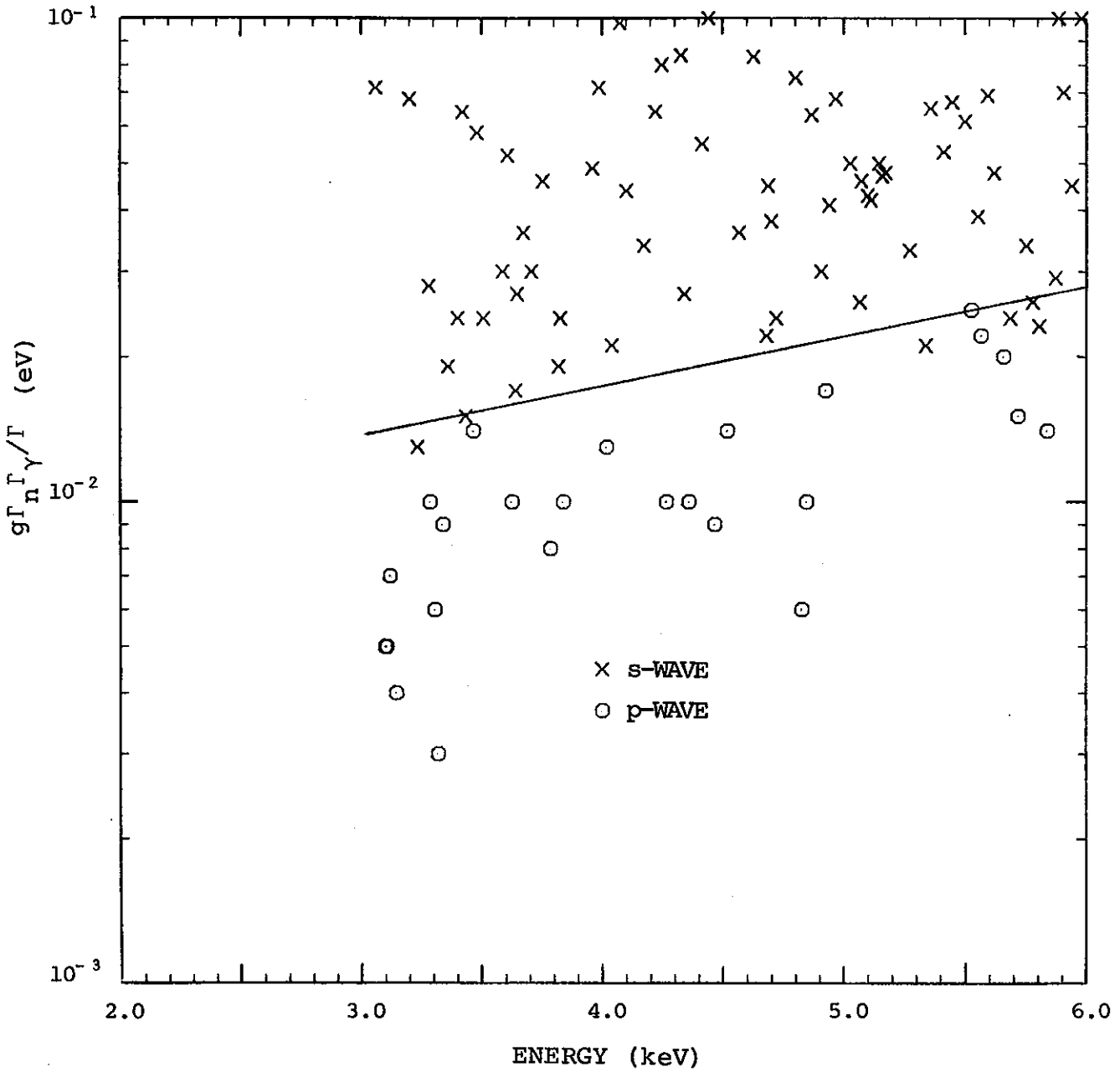

AAEC ℓ-WAVE ASSIGNMENTS ARE SHOWN WITH THE BOUNDARY CALCULATED FROM BAYES' THEOREM AT WHICH A LEVEL HAS EQUAL PROBABILITY FOR BEING s-WAVE OR p-WAVE

FIGURE 7. VALUES OF $g\Gamma_n\Gamma_\gamma/\Gamma$ FOR ALL LEVELS DETECTED VERSUS E

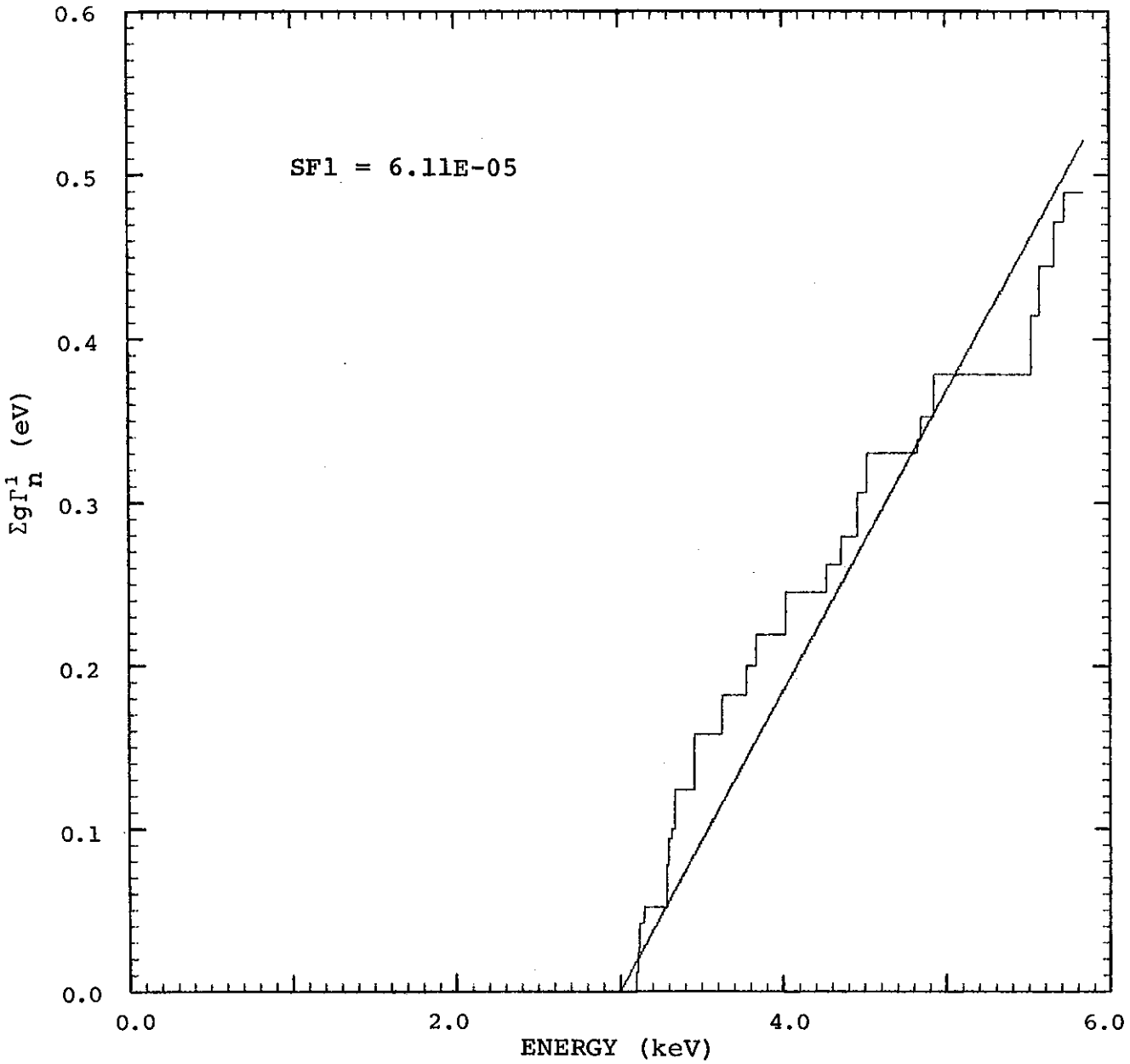

FIGURE 8. CUMULATIVE SUM OF $g\Gamma_n^1$ VERSUS E. THE SLOPE OF THE STRAIGHT LINE GIVES A p-WAVE STRENGTH FUNCTION OF 0.6×10^{-4}

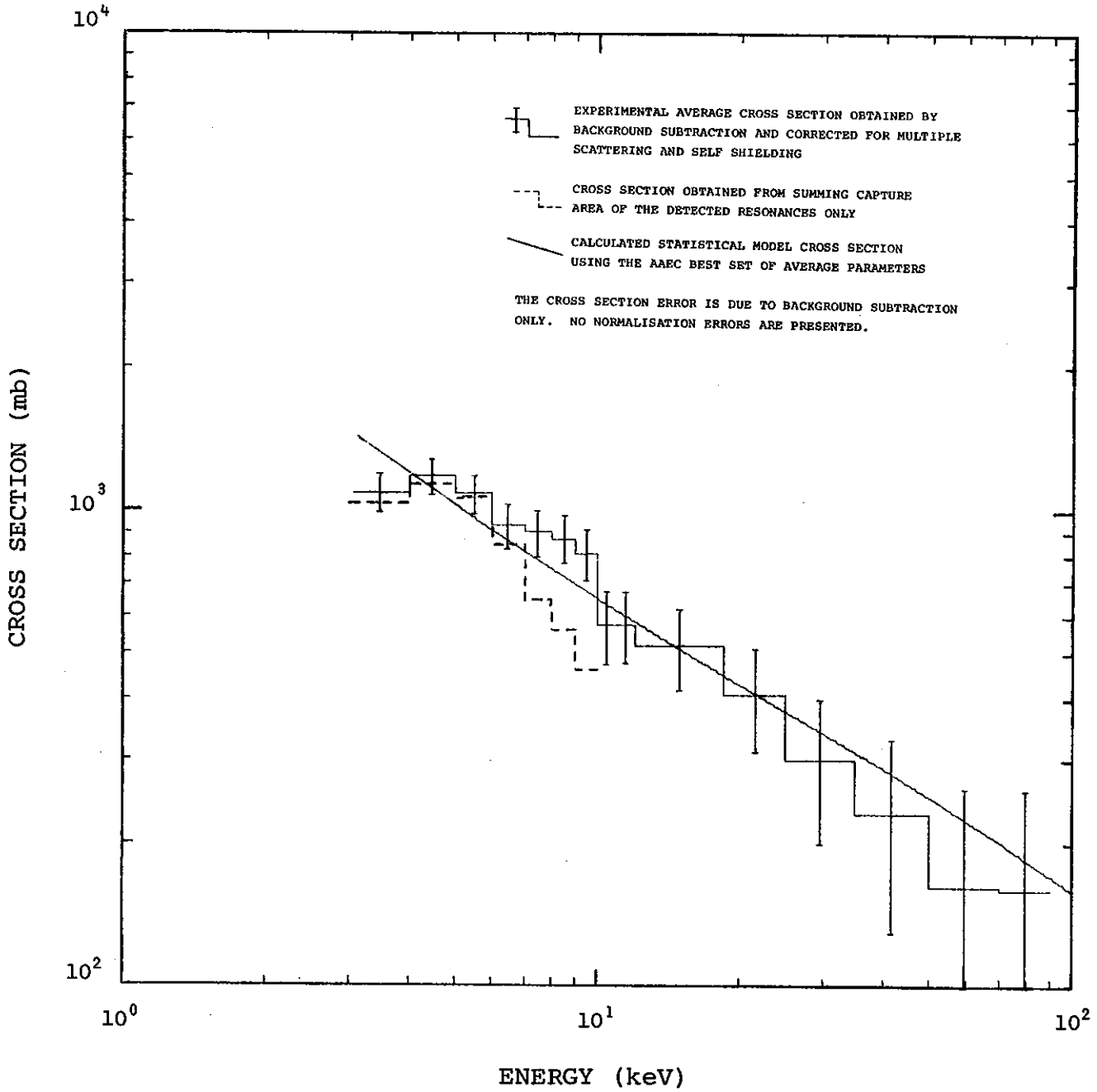

FIGURE 9. EXPERIMENTAL AND CALCULATED CROSS SECTIONS FOR ^{135}Ba